Codesign of an Impulse Generator and Miniaturized Antennas for IR-UWB

Sumit Bagga, *Student Member, IEEE*, Alexander V. Vorobyov, Sandro A. P. Haddad, *Student Member, IEEE*, Alexander G. Yarovoy, *Senior Member, IEEE*, Wouter A. Serdijn, *Member, IEEE*, and John R. Long, *Member, IEEE*

***Abstract*—The codesign of an impulse generator and miniaturized antennas for ultra-wideband impulse radio is described. The impulse generator, discussed by Bragga *et al.* in 2004, is designed with differential outputs that are fed to the antenna, producing an optimum match of the generator to the antenna, an improved magnitude response, and reduced ringing of the radiated pulse. The impulse generator is preceded by a programmable pulse-position modulator and consists of a triangular pulse generator and a cascade of complex first-order systems, which, in turn, are made up of differential pairs employing partial positive feedback to approximate a Gaussian monocycle waveform. The complete pulse generator is fabricated in IBM 0.18-μm Bi-CMOS IC technology. Measurements show the correct operation of the circuit for supply voltages of 1.8 V and a power consumption of 45 mW. The output pulse approximates the Gaussian monocycle having a pulse duration of about 375 ps. Proper modulation of the pulse in time is confirmed. A number of antennas with differentially fed baluns and input impedances of 100 Ω have been designed. From measurements, it can be seen that ringing is considerably smaller as compared to conventionally fed antennas.**

***Index Terms*—Antennas, impulse radio, integrated circuits (ICs), pulse-position modulation, transceiver, ultra-wideband (UWB).**

I. Introduction

IN TODAY'S marketplace for emerging communication technologies, the focal point of attention is ultra-wideband (UWB) radio, as it not only promises enhanced data throughput with low-power consumption, but also provides high immunity against electromagnetic interference (EMI) and robustness to fading. It is expected that future short-range indoor UWB telecommunication systems will operate in the frequency band from 3.1 to 10.6 GHz, according to the Federal Communications Commission (FCC) mask [2]–[5]. One form of UWB technology is *impulse radio*, in which information is transmitted by very short EM pulses [2], [6]. An impulse generator and special (so-called transient) antennas [7] are thereby employed in order to radiate these very short pulses. The codesign of the impulse generator and miniaturized antennas is the focus of this paper. Pulse-position modulation is used to encode the binary transmitted data [8], [9]. The waveform to be transmitted is the Gaussian monocycle due to its intrinsic time–frequency resolution product [6], [10], which is important for applications such as positioning and imaging. The impulse generator consists of a cascade of a fast triangular pulse generator and a Gaussian filter (i.e., a filter with a Gaussian impulse response) [11], [12]. The filter is implemented as a cascade of three complex first-order systems (CFOSs), which, in turn, consist of gm-C sections that employ differential pairs with partial positive feedback. The entire transmitter is the combination of the modulator with the impulse generator and the antenna (see Fig. 1).

The short transient pulses fired by the impulse generator must be properly transmitted by an antenna. This antenna must not only have an operational bandwidth of at least a few gigahertz within the stipulated frequency range, but also be able to radiate short pulses without substantial late-time ringing (i.e., oscillations in the radiated waveform after the main pulse). As a result, antennas for impulse radio are required to have a linear phase characteristic within the frequency band of operation.

In the design of an antenna, all physical as well as technical aspects must be taken into consideration, such as the feasibility of integrating small and flat (2-D) antennas into mobile devices. Moreover, as the antenna should be closely integrated with a transmitter and a receiver, it should be very well matched (i.e., achieve a voltage standing-wave ratio (VSWR) < 2 within the entire operational frequency band). The optimal solution would be to have antennas integrated on printed circuit boards (PCBs). Integration with RF circuits gives additional freedom in antenna design, as the antenna input impedance is not limited to 50 Ω. Balanced feeding can be realized without a balun by using a differential amplifier in the receiver and an impulse generator with a differential output in the transmitter. The desired radiation pattern of the antenna should be omnidirectional, and, to reduce power consumption of the entire system, the peak-to-peak magnitude of the radiated pulse is maximized. Finally, the antenna should be mounted on a dielectric substrate, which serves as a protective mechanical shield.

Among a number of impulse-radiating antennas recently developed for UWB communications, the dipole antenna with elliptically shaped flairs is a popular choice [13]. Even though this antenna exhibits a relatively low and flat input impedance over a large frequency range, the operational frequency band is smaller than the band in which the antenna is well matched to the feeding line. Furthermore, at higher frequencies, the operational frequency band is limited by a sharp decrease of the antenna gain (i.e., in bore sight direction) as a result of splitting

Manuscript received August 1, 2005; revised January 12, 2006.

S. Bagga, S. A. P. Haddad, W. A. Serdijn, and J. R. Long are with the Faculty of Electrical Engineering, Mathematics, and Computer Science, Electronics Research Laboratory, Delft University of Technology, 2628CD Delft, The Netherlands (e-mail: s.bagga@ewi.tudelft.nl; s.haddad@ewi.tudelft.nl; w.a.serdijn@ewi.tudelft.nl; j.r.long@ewi.tudelft.nl).

A. V. Vorobyov and A. G. Yarovoy are with the Faculty of Electrical Engineering, Mathematics, and Computer Science, International Research Centre for Telecommunications and Radar, Delft University of Technology, 2628CD Delft, The Netherlands (e-mail: a.vorobyov@ewi.tudelft.nl; a.yarovoy@ewi.tudelft.nl).

Digital Object Identifier 10.1109/TMTT.2006.872036

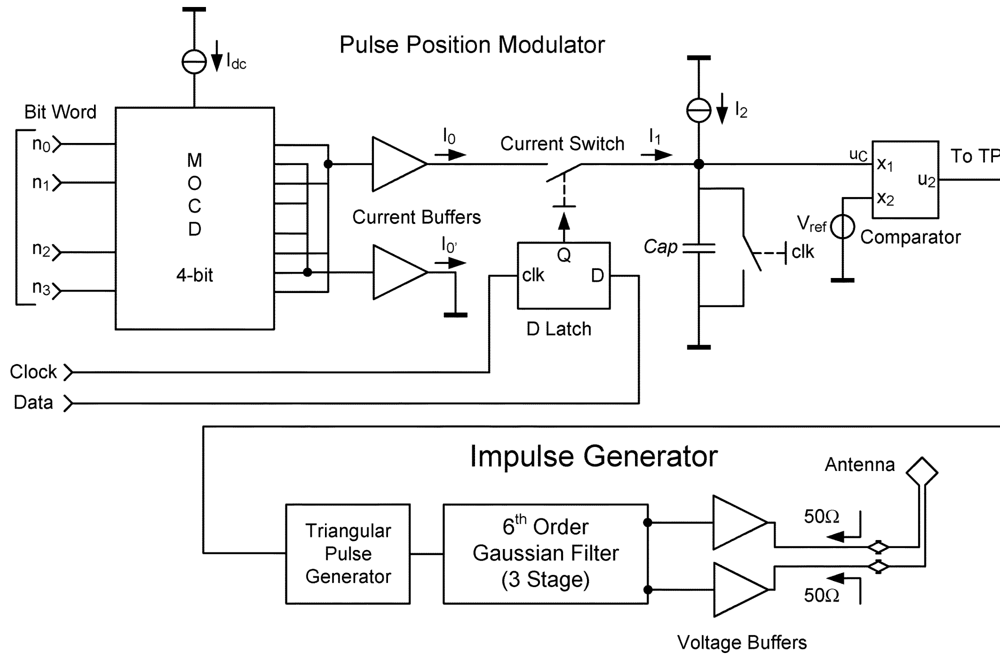

Fig. 1. Block diagram of impulse generator and modulator.

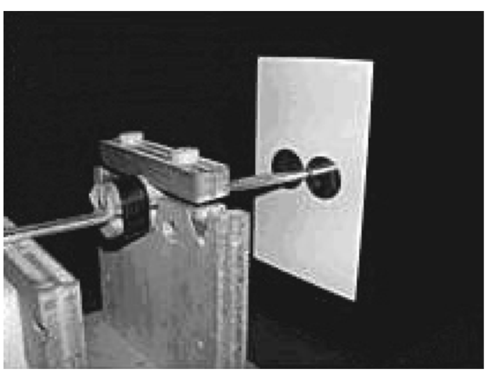

Fig. 2. Butterfly antenna for UWB communications.

the antenna radiation pattern into two lobes. Hence, the relative bandwidth of the antenna (i.e., based on the antenna gain) is slightly higher than one octave, which simply does not cover the entire frequency band approved by the FCC for UWB communications.

Relying on our past experience with elliptically shaped dipoles [14], we have developed a so-called butterfly antenna to be used in UWB communications [15]. This antenna is capable of radiating a 200-ps monocycle impulse that is sent from an impulse generator. The experimental antenna has been optimized for both Duroid 5870 as well as Rogers's 4003 substrates with a thickness of 0.8 mm. The dielectric permittivity of the 5870 and 4003 substrates is about 2.3 and 3.4, respectively, in the required frequency band. The optimized length of the butterfly antenna is about 2.2 cm, and the optimal flair ellipticity is 0.9 (see Fig. 2). The experimental antenna is fed by a double semirigid cable. Because of the finite diameter of the semirigid cable, the antenna flairs are separated by 3.2 mm. This antenna has been considered as a prototype for an integrated "*generator-antenna*" system.

In Section II, the design of the impulse generator and the modulator is discussed.

II. Impulse Generator and Modulator

Two possible combinations of a pulse-position modulator (PPM) and an impulse generator are considered. The delay circuit in the modulator used for pulse-position modulation can act upon incoming binary or continuous-time signals. Therefore, the modulator can be positioned either before or after the impulse generator. Delaying continuous-time signals requires a much higher degree of hardware complexity compared to delaying a binary signal. For this reason, the modulator is placed before the impulse generator, as shown in Fig. 1. In order to obtain pulse-position modulation, a ramp is generated, whose slope depends on the information signal [16], [17]. The ramp is then fed to the input of the comparator that compares the momentary value of the ramp with a fixed threshold and generates a trigger [18].

The PPM modulator comprises a 4-b MOSFET-only current divider (MOCD), which delivers a dc current (I_0) derived from its input code $\{n_0 \ldots n_3\}$ and I_{dc}, according to

$$I_0 = I_{\rm dc} \sum_{i=0}^{3} n_i 2^{(i-4)} u(t) \tag{1}$$

(see Fig. 1). The current switch conveys I_0 to I_1 only if its input bit is "high." The D-latch synchronizes the incoming binary data with the clock phase. As a result, when the incoming binary data is high as well as the clock phase, I_1 is added to I_2. Likewise, on a "low," only I_2 is used as the input to capacitance Cap. This capacitance acts as an integrator, generating a ramp signal voltage. The slope of the ramp depends on the total current [$I = I_1 + I_2$

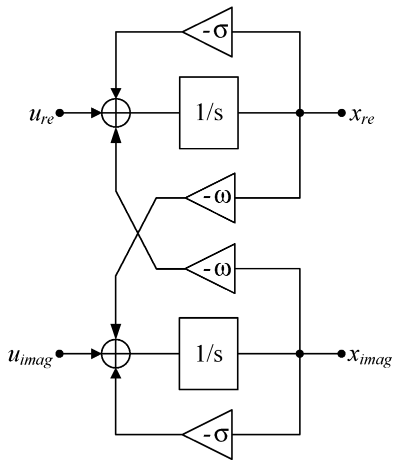

Fig. 3. CFOS block diagram.

(bit "1") or I_2 (bit "0")] through the capacitance, according to the well-known constitutive relation

$$u(t) = \frac{1}{\mathrm{Cap}} \int_0^t I(\tau) d\tau + u_c(t)|_{t=0}. \tag{2}$$

The output voltage of the capacitance u_C, in turn, is fed to the comparator that compares the momentary value of the ramp with a fixed threshold (V_{ref}) and generates an edge. This edge is then used to drive the triangular pulse generator, which consecutively triggers the impulse response of the succeeding pulse-shaping network, as it is a Gaussian filter.

A. Complex First-Order Filters

The Gabor transform [10] can be used to implement a Gaussian filter as its impulse responses are approximated Gaussian window functions, which are the first and second derivatives of Gaussian, respectively. The Gaussian filter can be implemented by a cascade of CFOSs. Gaussian monocycles have an excellent time–frequency resolution product, making them ideal for applications such as imaging and positioning.

A complex filter has a transfer function with complex-valued coefficients, which is not limited to complex-conjugate pairs of poles or zeros. A single-pole complex filter with a real axis coordinate σ and an imaginary axis coordinate ω has a transfer function given by

$$H(s) = \frac{V_{\mathrm{out}}(s)}{V_{\mathrm{in}}(s)} = \frac{1}{(s + (\sigma - j\omega))} = \frac{s + (\sigma + j\omega)}{(s+\sigma)^2 + \omega^2}. \tag{3}$$

A complex filter can be realized by means of cross-coupled real filters. Its structure exhibits similar characteristics as an ordinary second-order system. This representation, denominated CFOS, is given in Fig. 3. A CFOS is defined by the following set of equations:

$$\frac{d\,(x(t))}{dt} = (\sigma + j\omega)x(t) + (c_{\mathrm{re}} + jc_{\mathrm{imag}})u(t) \tag{4}$$
$$x(t) = x_{re}(t) + jx_{\mathrm{imag}}(t) \tag{5}$$

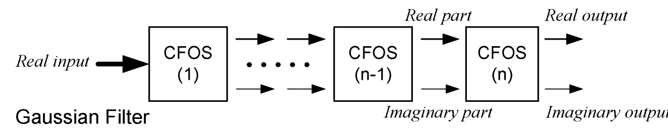

Fig. 4. Cascaded CFOS stages.

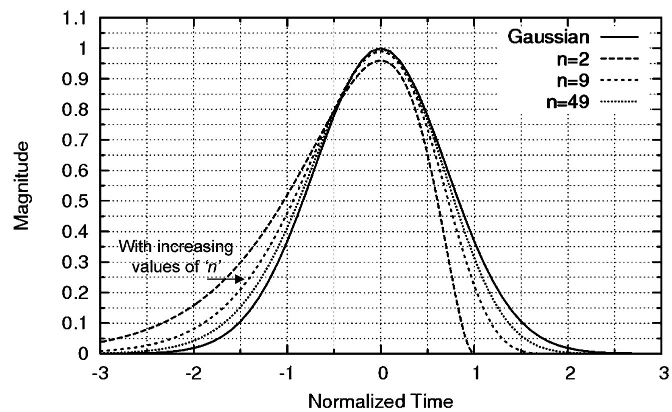

Fig. 5. Impulse response of a cascade of first-order systems with an increasing the number of stages.

where u is an input signal assumed to be real, x is a state variable assumed to be complex, and σ, ω, c_{re}, and c_{imag} are system parameters that are also assumed to be real. The real and imaginary parts of x, x_{re} and x_{imag}, respectively, can be described as

$$\frac{d(x_{\mathrm{re}})}{dt} = \sigma x_{\mathrm{re}} - \omega x_{\mathrm{imag}} + c_{\mathrm{re}} u \tag{6}$$
$$\frac{d(x_{\mathrm{imag}})}{dt} = \sigma x_{\mathrm{imag}} + \omega x_{re} + c_{\mathrm{imag}} u. \tag{7}$$

Subsequently, we can cascade CFOSs as shown in Fig. 4 in order to make a reasonable approximation to a Gaussian function. The envelope of the impulse response of these $(n+1)$ CFOS stages connected in cascade is given by [11]

$$h(t) = (c_{\mathrm{re}} + jc_{\mathrm{imag}})^{n+1} \frac{t^n}{n!} e^{\sigma t} U(t) \tag{8}$$

where $U(t)$ denotes a step unit function.

Equation (8) can also be defined as a Poisson function. Through statistical analysis, it is well known that, when $n! \to \infty$, the Poisson function approaches a Gaussian function. Therefore, by increasing the number of stages, one achieves a better approximation to the Gaussian function.

As one can see in Fig. 5, an improvement in the approximation to a Gaussian impulse response is obtained for a larger number of stages.

One can now easily calculate the general transfer function of an $(n+1)$ CFOS system for the real and the imaginary outputs, which are given as follows:

$$H_{\mathrm{re}}(n) = \frac{(s+\sigma)H_{\mathrm{re}}(n-1) - \omega H_{\mathrm{imag}}(n-1)}{(s+\sigma)^2 + \omega^2} \tag{9}$$
$$H_{\mathrm{imag}}(n) = \frac{(s+\sigma)H_{\mathrm{imag}}(n-1) + \omega H_{\mathrm{re}}(n-1)}{(s+\sigma)^2 + \omega^2} \tag{10}$$

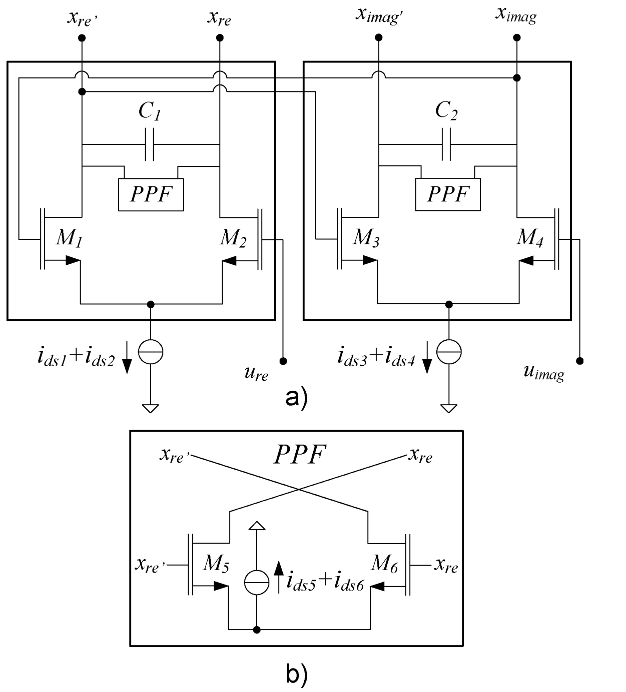

Fig. 6. (a) CFOS employing two differential pairs with gain enhancement by PPF. (b) Implementation of PPF.

$$H_{\mathrm{re}}(1) = \frac{s+\sigma}{(s+\sigma)^2+\omega^2} \tag{11}$$

$$H_{\mathrm{imag}}(1) = \frac{\omega}{(s+\sigma)^2+\omega^2} \tag{12}$$

in which $H_{\mathrm{re}}(1)$ and $H_{\mathrm{imag}}(1)$ correspond to the transfer function of the first-order complex filter. By choosing the right values for σ and ω, one can obtain the imaginary and the real part of the complex Gabor, respectively, for different numbers of stages.

In the next section, a cascade of three CFOS stages will be employed to approximate a Gaussian monocycle waveform. A three-stage filter is chosen after taking into account the tradeoff between power consumption and circuit complexity, on the one hand, and accuracy of the Gaussian monocycle on the other.

B. Circuit Design

In this section, the Gaussian filter, the triangular pulse generator, and the modulator circuits are discussed.

1) Gaussian Filter: A single CFOS stage using a differential pair arrangement with partial positive feedback (PPF) [19] is shown in Fig. 6. As expected, the inclusion of the PPF stage as active load enhancement not only increases the dc gain but also the unity gain frequency. The significant increase in gain and bandwidth is contributed to the increase in the effective transconductance of the stage. If L is the loop gain, then the gain of the amplifier is enhanced by a factor of $1/(1-L)$.

When L tends to 1, the gain tends to infinity. If L is made too large or too small, it will either make the system unstable or have little to no effect on the performance of the amplifier at all. Thus, L should be bounded, such that it has a lower and upper bound of 0 and 1, respectively. A significant improvement in the response time is seen due to the PPF loop. One could even use pMOS pull-ups as a positive feedback load to save power [19].

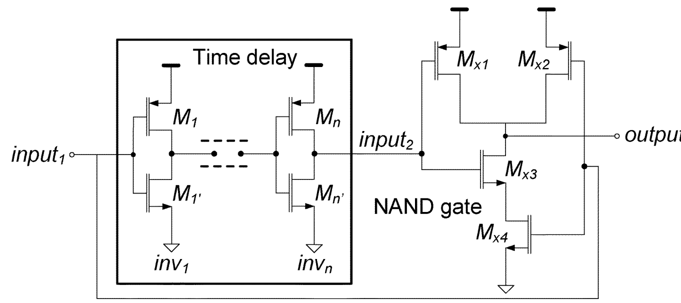

Fig. 7. Triangular pulse generator.

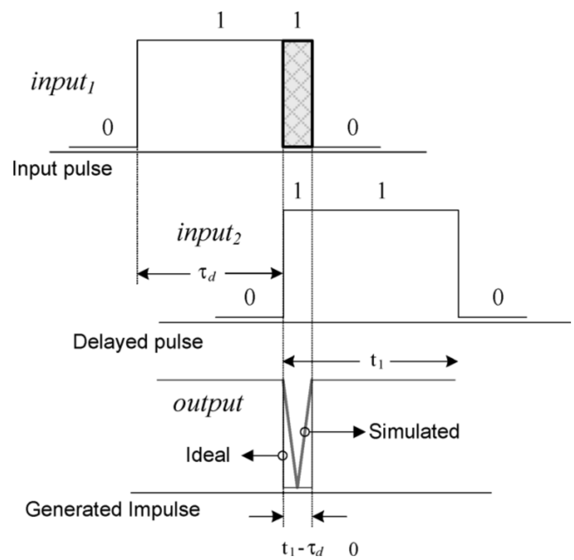

Fig. 8. Input and output waveforms of triangular pulse generator.

2) Triangular Pulse Generator: The triangular pulse generator is made up of a cascade of inverter stages, followed by a NAND gate function (see Fig. 7). The key purpose of this block is to generate an impulse-like function that is able to evoke the impulse response of the succeeding pulse-shaping network.

The input pulse $(input_1)$ and its delayed self $(input_2)$ act as two inputs to the NAND gate. Only when both inputs for a NAND gate are "high" is its output low. Hence, an impulse-like waveform is generated to drive the Gaussian filter, where its pulsewidth is approximately equal to the propagation delay of a single inverter times the total number of inverters (see Fig. 8).

3) Modulator Design: The schematic of the MOCD is shown in Fig. 9. The output currents of the MOCD are digitally programmable fractions of the applied input current I_{dc} [20]. To ensure correct operation, the two output nodes as shown in

$$I_0 = \sum_{i=0}^{3} I_{0i} \tag{13}$$

$$I_{0'} = \sum_{i=0}^{3} I_{0'i} = (I_{\mathrm{dc}} - I_0) \tag{14}$$

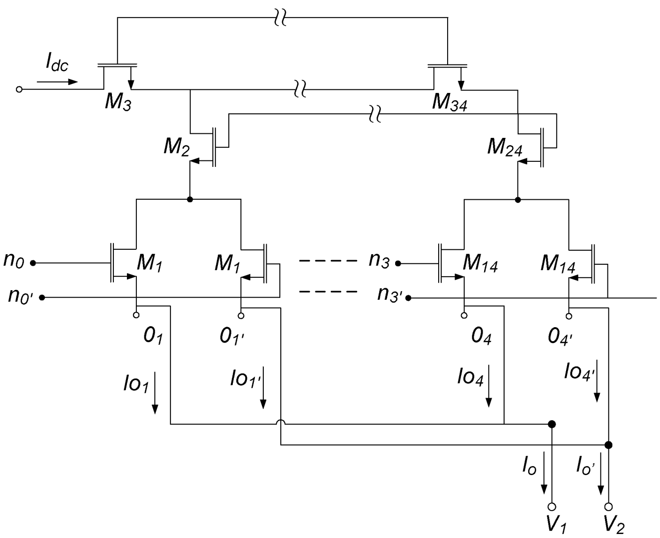

Fig. 9. 4-bit MOCD.

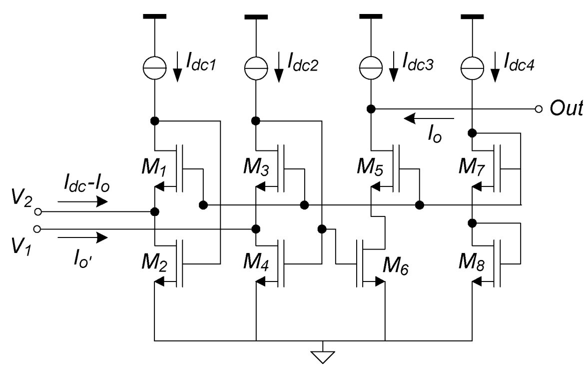

Fig. 10. Current buffer.

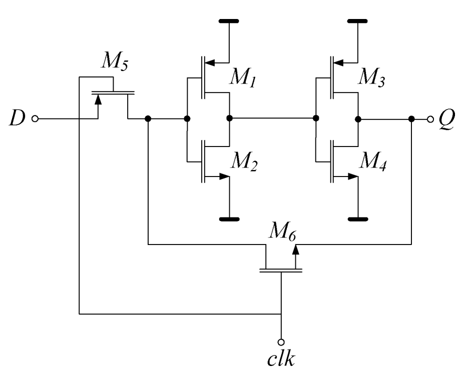

Fig. 11. D-latch.

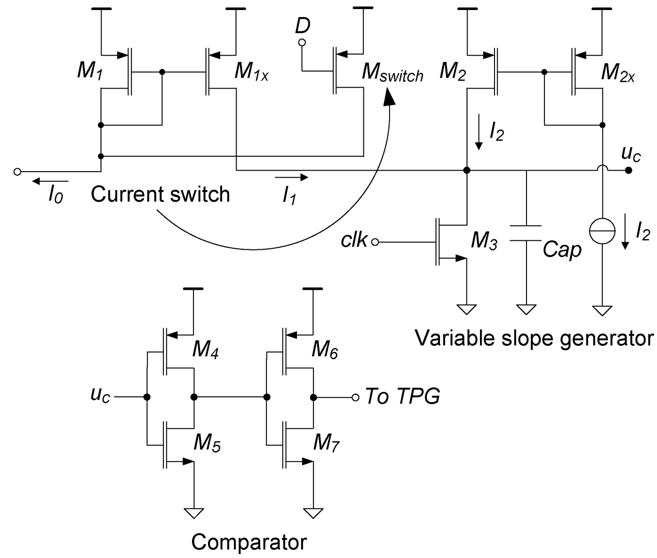

Fig. 12. Current switch, variable slope generator, and comparator.

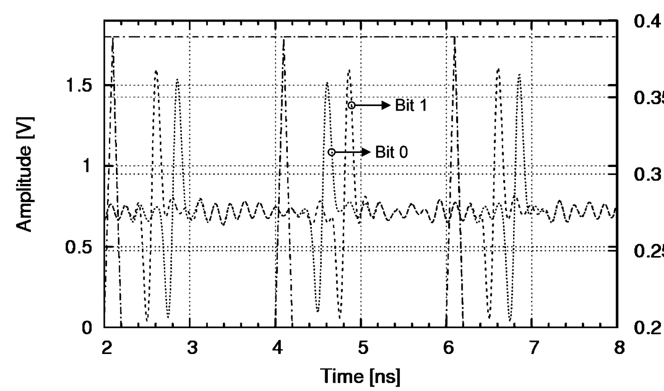

Fig. 13. Pulse-position modulation of Gaussian monocycle: bit 0 and bit 1.

have to be held at the same potential or, in other words, the potential at node V_1 should be equal to that at V_2. This condition necessitates two current buffers.

As shown in Fig. 10, the current buffer comprises of current sources ($I_{\rm dc1}$, $I_{\rm dc2}$, $I_{\rm dc3}$, and $I_{\rm dc4}$) delivering a reference current of $I_{\rm dc}$ and a cascode current mirror configuration (M_1, M_2, and M_3, M_4). M_6 mirrors the current $(I_{\rm dc} + I_0)$ and, in conjunction with the output of the D-latch, the output current I_0 is subsequently delivered to the current switch.

The binary data (i.e., the information) is fed to the input of the D-latch and is acquired by the latch as soon as the clock/phase goes high. Its circuit diagram is shown in Fig. 11.

As shown in Fig. 12, the current mirror formed by transistors M_1 and M_{1x} mirror the current I_o from current buffer to the variable slope generator in conjunction with the current switch $M_{\rm switch}$. The variable slope generator behaves as an intermediate between the preceding current buffers and the following comparator. As soon as the incoming binary data and the clock are high, I_1 is added to I_2. Likewise, on a "low," only I_2 is used as the input to capacitance Cap to generate a ramp. This resulting ramp serves as the input to the comparator, which makes a comparison of the momentary value of the ramp with a fixed threshold to generate an edge. Henceforth, this edge is used to drive the triangular pulse generator.

C. Simulation Results

The target of achieving 200-ps Gaussian pulses was not feasible because of the significant contribution of parasitic capacitances in 0.18-μm CMOS technology. The smallest possible pulsewidth attained was 250 ps before post-layout simulations and roughly 300 ps after layout extraction with amplitudes of 175 $\mathrm{mV}_{\rm pk-pk}$ (differential). The power consumption was approximately equal to 45 mW at a power supply of 1.8 V. Picosecond to nanosecond delays can be obtained by using this programmable delay circuit, as shown in Fig. 13.

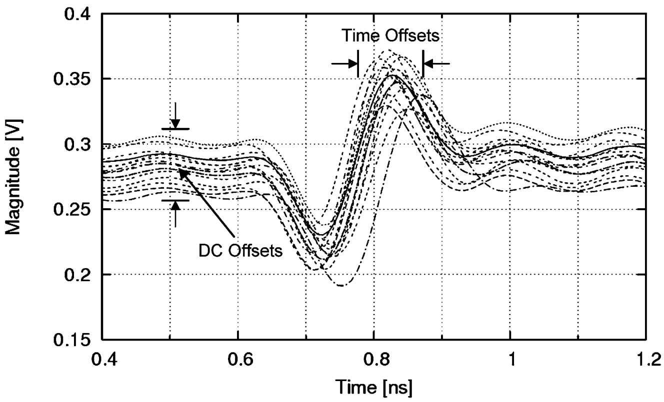

Fig. 14. Sensitivity analyses—Monte Carlo.

Finally, by randomly varying (i.e., 15 iterations) the component tolerances between their specified tolerance limits, a Monte Carlo analysis is run in order to estimate the circuit's sensitivity. From Fig. 14, it is inferred that the Gaussian monocycle is relatively unlikely to show a substantial discrepancy as a result of process and mismatch variations. Variations in dc levels can be tolerated as long as the shape is preserved.

III. Antenna Design

A. Theoretical Model

In designing the antenna and optimizing its performance, we developed a computational model using the commercial EM simulator FEKO [21], which is based on the volumetric mixed-potential integral equation (MPIE) formulation. Within the model, the finite dielectric substrate is subdivided into cuboids. Each element can be assigned a different material property. Inside each cuboid element, the polarization current is assumed to be unknown. The antenna flairs, which are assumed to be perfectly conducting and infinitely thin, are modeled by a surface current and are subdivided into triangular surface elements. The Rao–Wilton–Glisson (RWG) basis functions are applied to these elements for the equivalent electric and equivalent magnetic surface currents. Boundary conditions on a surface of metal in method of moments (MoM) are carried out approximately, e.g., in several points within the limits of each elementary patch (strictly, these conditions should be carried out in all points). The integral equation is solved by the MoM. As a reference model (for the case of free space and for the antenna on an infinite substrate), we have used a model based on the surface MPIE. The impact of the infinite substrate is taken into account by the proper Green functions in the kernels of the integral equations.

From a system designer's point of view, both the antenna and an impulse generator should be integrated on a PCB, with the latter being placed between the antenna flairs. This is why the feeding line is not included into our numerical model. The antenna is excited by passing a current through the wire between the antenna flairs. The waveform that is fed to the antenna by the generator is assumed to be the Gaussian monocycle with a pulse duration of approximately 0.2 ns. The spectral content of the pulse is already insignificant (i.e., slightly higher than -40 dB with respect to the maximum) at 20 GHz. Simulation results in the frequency domain over 101 frequencies from 0.20 to 20 GHz have been performed. To improve the time-domain resolution, we applied zero padding, thus expanding the frequency range up to 49.4 GHz. Together with proper windowing in the frequency domain and the inverse Fourier transform for calculating the radiated field in time domain, this approach allows us to perform a fast and accurate time-domain analysis of antennas with arbitrary shaped metal flairs on a dielectric structure.

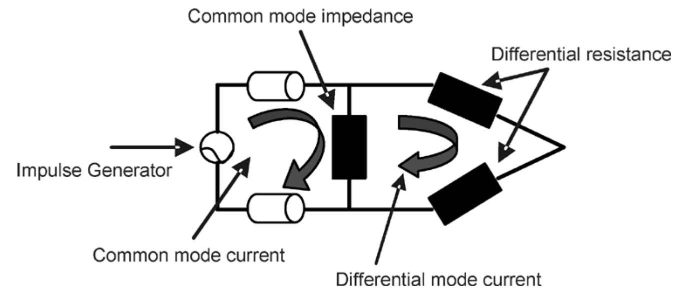

Fig. 15. Excitation of the common-mode and differential-mode currents.

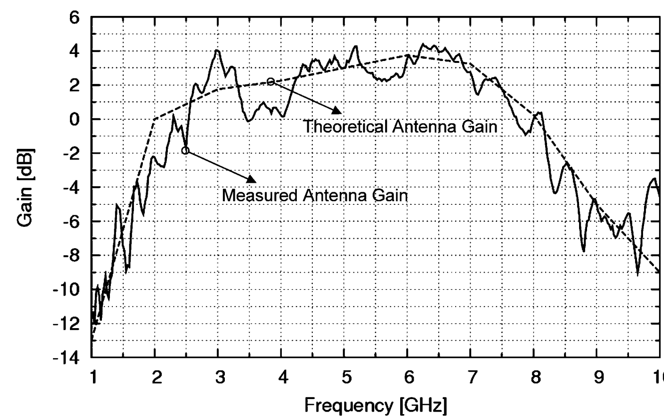

Fig. 16. Antenna gain versus frequency: theory and experimental.

B. Common-Mode Current and Balun Design

Large common-mode currents were present on the feeding cables during the experimental verification of the prototype design (see Fig. 2). The common-mode current and its excitation are explained by Fig. 15. For any symmetrical antenna fed via a conventional asymmetrical feeding line (e.g., a semirigid cable), the current received from the generator is divided into two components: the differential-mode current and the common-mode current. The former excites the antenna while the latter propagates along the outer surface of the feeding line and causes parasitic radiation. The relative magnitude of the current components is determined by the ratio of the common-mode and differential-mode antenna impedances.

As a result of the common-mode current, the antenna gain in the boresight direction oscillates with frequency (see Fig. 16). The antenna radiation patterns also show an oscillatory behavior.

In order to avoid excitation of the common-mode current, we developed a UWB balun. This antenna-feed circuit design (see Fig. 17) is based on the shielded loop [22]. The semirigid coaxial

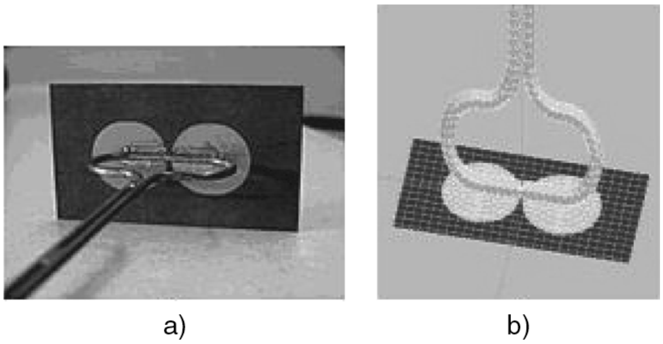

Fig. 17. (a) Butterfly antenna with loop feed circuit photograph. (b) Computational model.

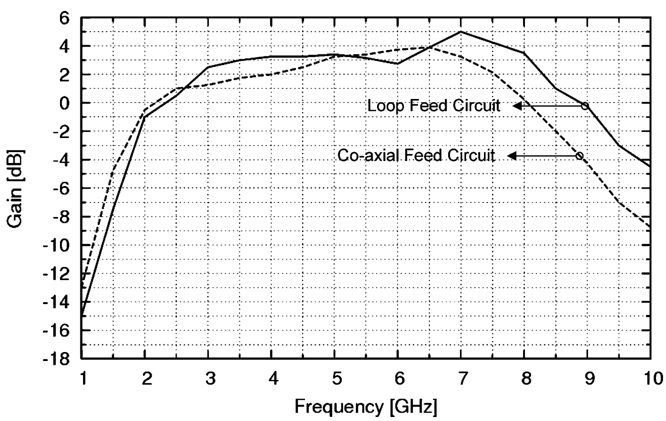

Fig. 18. Antenna gain for two feeding circuits.

feeding cable (which is a 50-Ω coaxial cable 2.1 mm in diameter) is bent into a loop shape. The cable is electrically connected to the antenna flairs. A small slot is made in the outer conductor of the cable right against the feeding slot between the antenna flairs. Now, to feed the antenna from a conventional generator, we only require one coaxial input, while the second is loaded by a dummy.

With regard to the size of the loop, a tradeoff can be made between the antenna gain, reflection coefficient, and common-mode impedance. By enlarging the diameter of the loop, the antenna gain decreases, whereas the reflection coefficient increases. In contrast, by reducing the loop diameter, one decreases the common-mode impedance. Through simulations, the dimension of the loop is made to vary from 11 to 24 mm and a loop with an 11-mm diameter and 1-mm slot was chosen. To avoid the antenna being loaded by the loop, the flair shape as well as size were adjusted for the best possible performance. If this step were omitted, the input impedance and the radiation performance would significantly differ from the expected values.

Comparison of the antenna gain for two antenna designs (i.e., with and without a balun) is shown in Fig. 18. It can be seen that the balun enlarges the antenna bandwidth by approximately 1 GHz due to better radiation at frequencies above 6.5 GHz.

The theoretical design of the antenna with a balun is experimentally verified by Fig. 19. The performance is extremely satisfactory as a result of the antenna being closely matched to the generator.

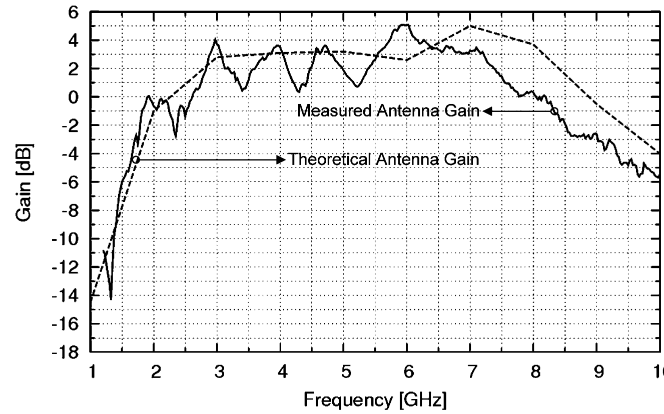

Fig. 19. Antenna gain for butterfly antenna with a loop-feeding line.

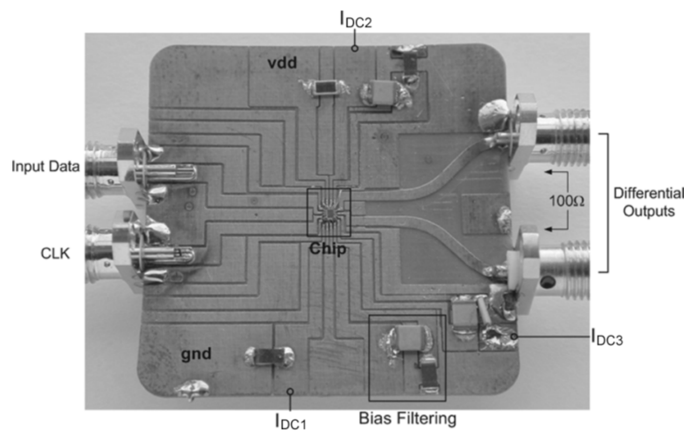

Fig. 20. Photograph of the chip wire-bonded to a test PCB.

IV. Measurements

A. Integrating the Antenna to the Impulse Generator

In this section, we investigate the integration of the antenna with the impulse generator. First, the chip is mounted on a PCB to be integrated with different antennas (see Fig. 20). In Fig. 21, the dimensions of the chip are given.

Bias filtering is used to prevent ESD that may damage the chip. The outputs are coupled via strip lines to the feeding line of the transmitting antenna.

The output waveforms from the impulse generator are measured using the setup shown in Fig. 22. The reference current $(I_{\rm dc})$ fed to the MOCD is set to 1 mA at a power supply of 1.8 V. Fig. 23 shows the measured Gaussian monocycle waveforms. Furthermore, to verify pulse-position modulation (see Fig. 24), a clock signal (1–5 MHz), which acts as the binary input signal, is streamed into the D-latch. A bit code (0001) is chosen to verify that the least significant bit would vary the position of the pulse by approximately 315 ps (i.e., for $I_1 = 0.625$ mA). Table I highlights the measured parameters of the impulse generator. The pulse widths obtained after post-layout simulation and those measured differ only by 75 ps.

The measurement parameters of the transmitter are given in Table I.

All measurements were carried out using a TEM-horn antenna as the receiving antenna placed approximately 35 cm from

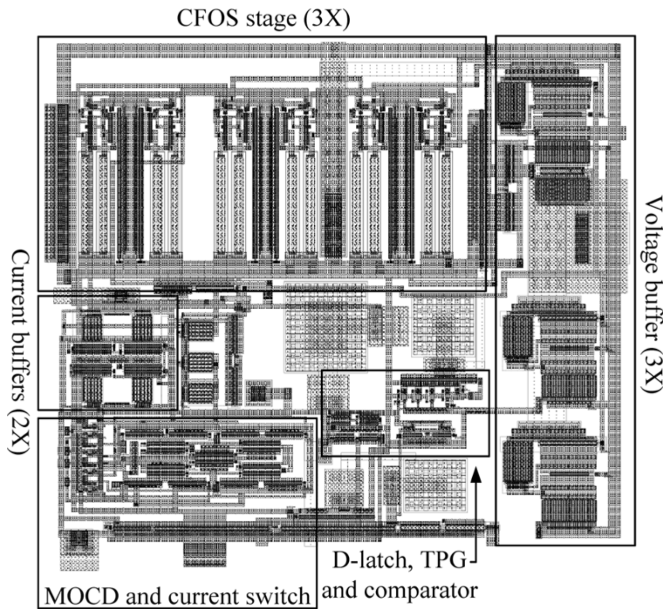

Fig. 21. Layout of impulse generator and modulator; the die area is 1.225 mm^2 ($1267\ \mu$m $\times$ $0.967\ \mu$m); the active area is 0.306 mm^2 (175 μm $\times$ 175 μm).

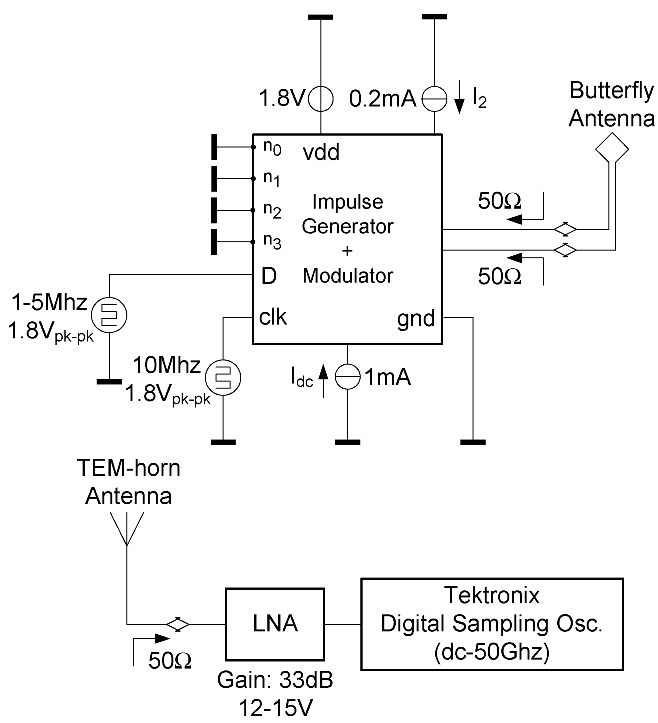

Fig. 22. Measurement setup.

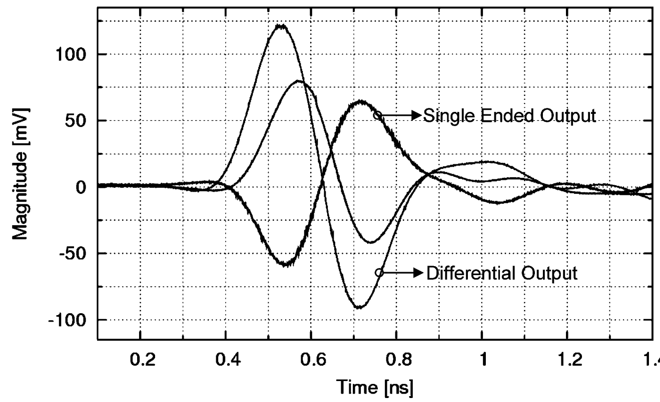

Fig. 23. Gaussian monocycle and differential output.

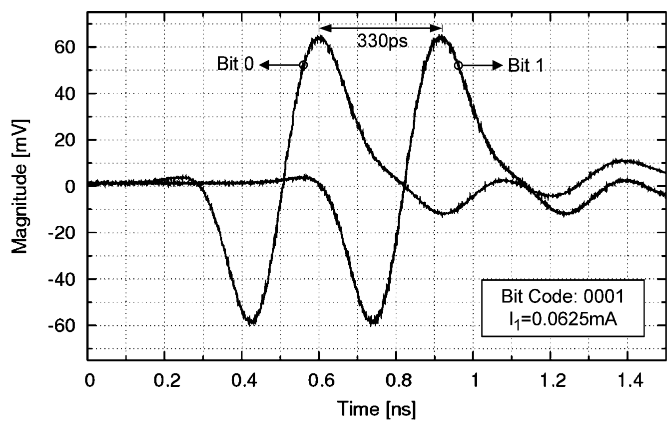

Fig. 24. Pulse-position modulation for bit code 0001.

TABLE I
MEASUREMENT PARAMETERS

Specifications	Measured
Pulse width Gaussian Monocycle	300ps–extracted (with bond wires) 375ps–measured on PCB
Time delay Bit code: 0001	330ps
Current consumption of Gaussian filter	14.4mA @ 1.8V
Differential Amplitude	$175mV_{pk-pk}$
Chip Size	1.225mm^2
Antennas	*TX*-Butterfly with & without a balun *RX* -TEM-horn
Distance between *TX* and *RX* antenna	35cm
Process	IBM Bi-CMOS 0.18μm

the transmitting antenna. Properly designed TEM-horn antennas faithfully reproduce waveforms of the received pulse as their transfer function is flat in the operational frequency band [23]. The TEM-horn [24], used in the experiments, has a flat receive transfer function in the frequency band from 1 to 4.8 GHz. At the frequencies from 4.8 to 10.6 GHz, the transfer response slightly decreases with frequency.

In Fig. 25, both inputs of the loop are fed from differential outputs of the impulse generator and, thus, the antenna is fed differentially.

Figs. 26 compares the radiated waveform from the differentially fed butterfly antenna with the measured differential waveform from the generator.

Because of the longer than expected (375 instead of 200 ps) waveform being fed to the antenna, the electrical size of the antenna is smaller than optimal and, as a consequence, the magni-

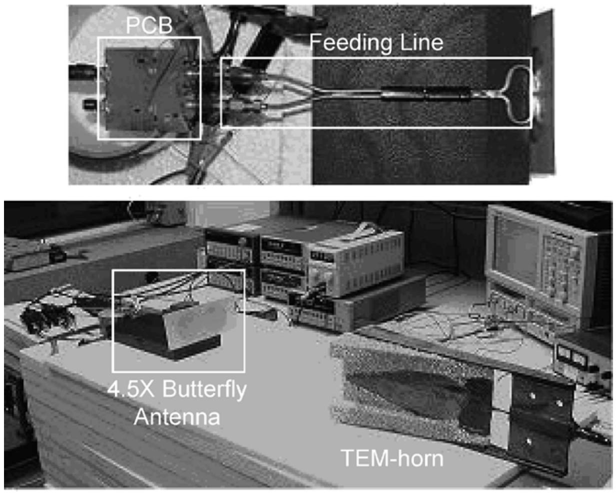

Fig. 25. Butterfly antenna with loop-feeding line connected to the differential generator.

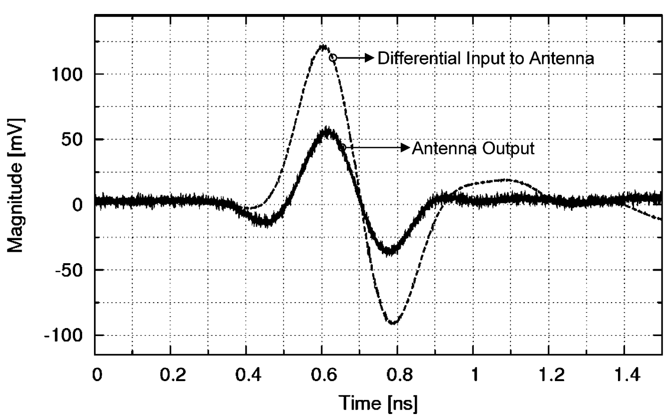

Fig. 26. Waveform (i.e., with 100-Ω load) versus waveform transmitted by a butterfly antenna.

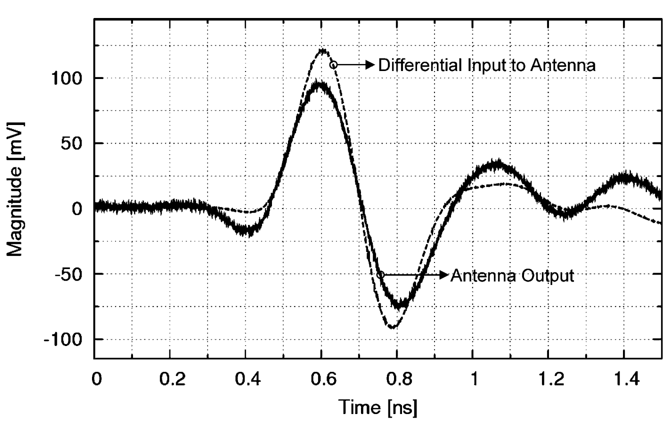

Fig. 27. Waveform (i.e., with 100-Ω load) versus waveform transmitted by a butterfly antenna (scaled-up version).

tude of the radiated pulse is smaller than expected. A scaled-up version of the antenna (4.5$\times$) radiates a 1.6$\times$ larger waveform (see Fig. 27), but with substantial ringing.

The balun increases the peak-to-peak magnitude of the radiated pulse and decreases ringing of the radiated pulse. In Fig. 28, the radiation of the similar butterfly antennas with and without a balun is compared.

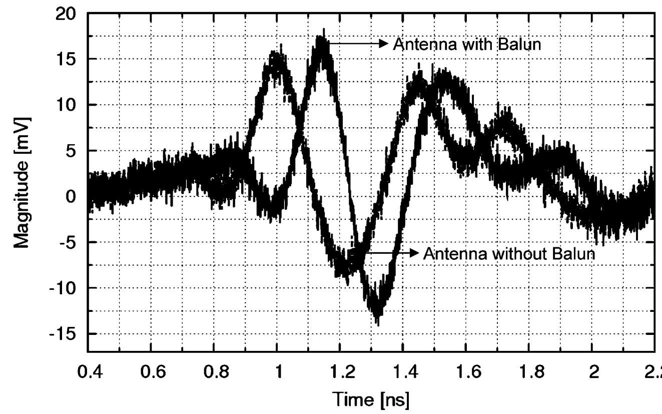

Fig. 28. Comparison of the radiated waveform from a butterfly antenna with and without a balun.

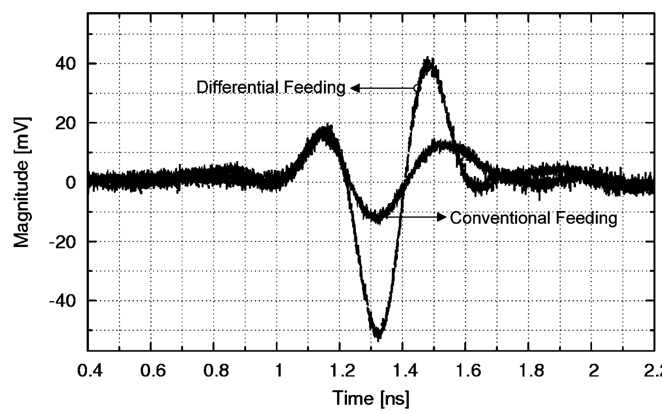

Fig. 29. Radiated waveform: conventionally fed versus differentially fed butterfly antenna.

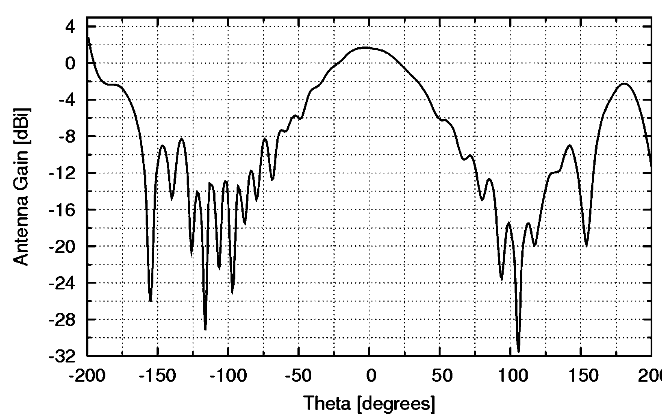

Fig. 30. Radiation pattern of a differentially fed antenna at 5 GHz.

Fig. 29 shows that, through differential feeding of the antenna, ringing can be significantly reduced.

In particular, when the common-mode current is suppressed, the radiation patterns become symmetrical (see Fig. 30), and the observed antenna ringing is considerably smaller as compared with an antenna without a balun.

V. Conclusion and Discussions

The codesign of an impulse generator and miniaturized antennas for UWB impulse radio is investigated. A fully programmable on-chip Gaussian monocycle generator incorporating a PPM for use in an impulse radio UWB system has been presented. Proper modulation of the information as well as an excellent approximation of the Gaussian monocycle has been achieved. The design is fabricated in 0.18-μm CMOS technology. A minimum pulsewidth of about 375 ps is attainable.

Moreover, the combination of a generator with differential outputs and an antenna with a differential feeding results in optimal solution of a number of problems. All the antennas designed have an input impedance of 100 Ω and are matched to the impulse generator.

The next step in such a codesign will be to integrate the antenna with the generator on the same PCB. This gives a number of further advantages, e.g., allowing a complex input impedance of the antenna. With respect to the generator, it is now possible to design a filter whose impulse response is a tailor-made waveform with a frequency response that follows the frequency mask stipulated by the FCC [25], [26].

Acknowledgment

The authors would like to thank D. Harame and IBM Microelectronics for fabrication access. They also thank W. Straver, J. Zijderveld, and P. Hakkaart for their outstanding technical support and R. Pugliese for the design of the butterfly antenna prototypes.

References

[1] S. Bagga, W. A. Serdijn, and J. R. Long, "A PPM Gaussian monocycle transmitter for ultra-wideband communications," in *Proc. Joint UWBST & IWUWBS*, May 2004, pp. 130–134.

[2] FCC 02-48—Federal Communication Commission, First Report and Order Regarding Ultra Wideband Transmission System [Online]. Available: http://www.fcc.gov adopted: Feb. 14, 2002, released: Apr. 22, 2002

[3] D. Porcino and W. Hirt, "Ultra-wideband radio technology: potential and challenges ahead," *IEEE Commun. Mag.*, vol. 41, no. 7, pp. 66–74, Jul. 2003.

[4] L. Yang and G. B. Giannakis, "Ultra-wideband communications: An idea whoes time has come," *IEEE Signal Process. Mag.*, vol. 21, no. 76, pp. 26–54, Nov. 2004.

[5] M. Z. Win and R. A. Scholtz, "Impulse radio: How it works," *IEEE Commun. Lett.*, vol. 2, no. 2, pp. 36–38, Feb. 1998.

[6] S. Roy, J. R. Foerster, V. S. Somayazulu, and D. G. Leeper, "Ultrawideband radio design: The promise of high-speed, short-range wireless connectivity," *Proc. IEEE*, vol. 92, no. 2, pp. 295–311, Feb. 2004.

[7] A. Yarovoy, "Ultra-wideband systems," in *Proc. 33rd Eur. Microw. Conf.*, Munich, Germany, 2003, pp. 597–600.

[8] H. G. Schantz, "A brief history of ultra wideband antennas," *IEEE Aerosp. Electromagn. Syst. Mag.*, vol. 19, no. 4, pp. 22–26, Apr. 2004.

[9] R. A. Scholtz, "Multiple access with time-hopping impulse modulation," in *Proc. MILCOM*, Oct. 11–14, 1993, vol. 2, pp. 447–450.

[10] X. Chen and S. Kiaei, "Monocycle shapes for ultra wideband system," in *Proc. IEEE Int. Symp. Circuits Syst.*, 2002, vol. 1, pp. 597–600.

[11] H. Kanada and N. Aoshima, "Analog Gabor transform filter with complex first order system," in *Proc. SICE*, 1997, pp. 925–930.

[12] J. M. Wilson, "Ultra-wideband/a disruptive RF technology?," *Version 1.3, Intel Research and Development*, Sep. 10, 2002.

[13] H. G. Schantz, "Planar elliptical element UWB dipole antennas," in *Proc. IEEE Antennas Propag. Soc. Int. Symp.*, 2002, vol. 3, pp. 44–47.

[14] R. V. de Jongh, A. G. Yarovoy, L. P. Ligthart, I. V. Kaploun, and A. D. Schukin, "Design and analysis of new GPR antenna concepts," in *Proc. 7th Int. Conf. Ground-Penetrating Radar*, Lawrence, KS, 1998, vol. 1, pp. 81–86.

[15] A. G. Yarovoy, R. Pugliese, J. R. Zijderveld, and L. P. Ligthart, "Antenna development for UWB impulse radio," in *Proc. 34th Eur. Microw. Conf.*, Amsterdam, The Netherlands, 2004, pp. 1257–1260.

[16] H. C. Morgan and W. H. Boyd, "Transmission of electronic information by pulse position modulation utilizing low average power," U.S. Patent 5 586 145, Dec. 17, 1996.

[17] M. Saint-Laurent and M. Swaminathan, "A digitally adjustable resistor for path delay characterization in high-frequency microprocessors," in *Soutwest Mixed Signal Des. Symp.*, Feb. 2001, pp. 61–64.

[18] E. W. Justh and F. J. Kub, "Analogue CMOS continuous-time tapped delay line circuit," *Electron. Lett.*, vol. 31, no. 21, Oct. 1995.

[19] R. Wang and R. Harjani, "Partial positive feedback for gain-enhancement of low-power CMOS OTAs," *Analog Integr. Circuits Signal Process.*, no. 8, pp. 21–35, 1995.

[20] K. Bult and G. J. G. M. Geelen, "An inherently linear and compact MOST-only current division technique," *IEEE J. Solid-State Circuits*, vol. 27, pp. 1730–1735, Dec. 1992.

[21] *"FEKO manual,"* [Online]. Available: http://www.feko.info

[22] J. J. Goedbloed, *Electromagnetische compatibiliteit; Analyze en underbrukking van stoorproblemen*. Deventer, Germany: Kluwer, 1990.

[23] P. R. Foster, "Antennas and UWB signals," in *Introduction to Ultra-Wideband Radar Systems*. Boca Raton, FL: CRC, 1995.

[24] A. G. Yarovoy, J. H. Zijderveld, A. D. Schukin, I. V. Kaploun, and L. P. Ligthart, "Dielectric wedge antenna for UWB applications," in *Proc. IEEE Int. Conf. Ultra-Wideband*, Zurich, Switzerland, Sep. 2005, pp. 186–189.

[25] S. A. P. Haddad, S. Bagga, and W. A. Serdijn, "Log-domain wavelet bases," in *Proc. IEEE Int. Symp. Circuits Syst.*, May 2004, pp. 1100–1103.

[26] S. Bagga, S. A. P. Haddad, K. van Hartingsveldt, S. Lee, and W. A. Serdijn, "An interference rejection filter for an ultra-wideband quadrature downconversion autocorrelation receiver," in *Proc. IEEE Int. Symp. Circuits Syst.*, May 2005, pp. 5357–5360.

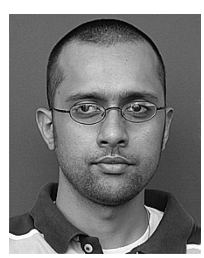

Sumit Bagga (S'03) was born in New Delhi, India, in 1977. He received the B.S. (with distinction) from Shivaji University, Kolhapur, India, in 1999, and M.Eng. degree from the University of Brasilia, Brasilia, Brazil in 2002, both in electrical engineering

In November 2002, he joined the Electronics Research Laboratory (ELCA-EEMCS), Delft University of Technology, Delft, The Netherlands, where he is involved with designing transceiver architectures and circuits for ultra-wideband (UWB) communications in the Ad hoc Impulse Radio: Local Instantaneous Networks (AIR-LINK) project under the FREEBAND initiative. His research interests include high-speed, low-power analog integrated circuits for RF and UWB wireless communications.

Mr. Bagga was the recipient of the Best Paper Award from UWBST and IWUWBS 2004.

Alexander V. Vorobyov received the M.S. degree in radiophysics and electronics from Kharkov State University, Kharkov, Ukraine, in 2000 , and he is currently working toward the Ph.D. degree at the Delft University of Technology, Delft, The Netherlands.

In 2002–2003, he was with the Department of Applied Mechanics, Kharkov Academy of Fire Safety, as an Assistant Lecturer. He was also involved with remote sensing of natural raw materials with respect to centers of self-warming up. In 2004, he joined the International Research Centre for Telecommunications-Transmission and Radar, Delft University of Technology. His main research interests are in applied electromagnetics, in particular, in design, miniaturization, and optimization of ultra-wideband antennas for telecommunications.

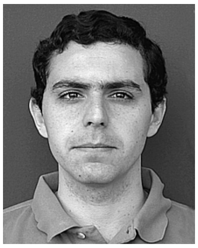

Sandro A. P. Haddad (S'99) was born in Annapolis, Brazil, in 1977. He received the B.Eng. degree (with honors) from the University of Brasilia, Brasilia, Brazil, in 2000, and he is working toward the Ph.D. degree at the Delft University of Technology, Delft, The Netherlands.

His research is a part of the Biomedical Signal Processing Platform for Low-Power Real-Time Sensing of Cardiac Signals (BioSens). His research interests include low-voltage, ultralow-power analog electronics and biomedical systems and high-frequency analog integrated circuits for ultra-wideband communications.

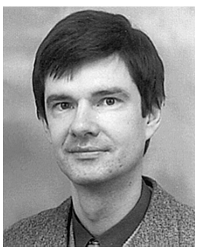

Alexander G. Yarovoy (M'95–SM'04) received the Cand. Phys. and Math. Sci. and Dr. Phys. and Math. Sci. degrees in radiophysics from Kharkov State University, Kharkov, Ukraine, in 1987 and 1994, respectively.

In 1987, he joined the Department of Radiophysics, Kharkov State University, as a Researcher and became a Full Professor in 1997. From September 1994 through 1996, he was with the Technical University of Ilmenau, Ilmenau, Germany, as a Visiting Researcher. Since 1999, he is with the International Research Centre for Telecommunications-Transmission and Radar, Delft University of Technology, Delft, The Netherlands, where he coordinates all UWB-related projects. His main research interests are in ultra-wideband (UWB) technology and its applications (in particular, UWB radars) and applied electromagnetics (in particular, UWB antennas).

Prof. Yarovoy served as the Co-Chairman and the Technical Program Committee Chair of the Tenth International Conference on Ground Penetrating Radar (GPR2004), Delft, and the Secretary of the 1st European Radar Conference (EuRAD'04), Amsterdam, The Netherlands.

Wouter A. Serdijn (M'98) was born in Zoetermeer, The Netherlands, in 1966. He received the ingenieurs (M.Sc.) degree and Ph.D. degree from the Delft University of Technology, Delft, The Netherlands, in 1989 and 1994, respectively.

His research interests include low-voltage, ultralow-power, high-frequency, and dynamic-translinear analog integrated circuits along with circuits for RF and ultra-wideband (UWB) wireless communications, hearing instruments, and pacemakers. Since 2002, he has been a Work Package Leader with the Freeband Impulse project AIR-LINK, aiming at high-quality, wireless short-distance communication, employing UWB radio. He is a coeditor and coauthor of the books *Research Perspectives on Dynamic Translinear and Log-Domain Circuits* (Kluwer, 2000), *Low-Voltage Low-Power Analog Integrated Circuits* (Kluwer, 1995), and *Dynamic Translinear and Log-Domain Circuits* (Kluwer, 1998). He has authored and coauthored more than 150 publications and presentations. He teaches analog electronics, micropower analog ic design and electronic design techniques.

Dr. Serdijn has served as an Associate Editor for the IEEE TRANSACTIONS ON CIRCUITS AND SYSTEMS I—REGULAR PAPERS, as an Associate Editor for the IEEE TRANSACTIONS ON CIRCUITS AND SYSTEMS II—EXPRESS BRIEFS, as tutorial session co-chair for ISCAS'2003, as Analog Signal Processing Track Co-Chair for ISCAS'2004, as chair of the Analog Signal Processing Technical Chapter of the IEEE CAS society, as Analog Signal Processing Track Co-Chair for ICECS'2004, as Technical Program Committee member for the 2004 International Workshop on Biomedical Circuits and Systems, as Analog Signal Processing Track Co-Chair for ISCAS'2005, and as International Program Committee member for IASTED CDD'2005, and currently (again) serves as an Associate Editor for the IEEE TRANSACTIONS ON CIRCUITS AND SYSTEMS I and as a member of the Board of Governors of the Circuits and Systems Society. In 2001 and 2004, he was the recipient of the EE Best Teacher Award.

John R. Long (S'77–M'83) received the B.Sc. degree in electrical engineering from the University of Calgary, Calgary, Canada, in 1984, and the M.Eng. and Ph.D. degrees in electronics from Carleton University, Ottawa, ON, Canada, in 1992 and 1996, respectively.

He was with by Bell-Northern Research, Ottawa (now Nortel), for ten years, where he was involved with the design of ASICs for Gb/s fiber-optic transmission systems and for five years as an Assistant and then Associate Professor with the University of Toronto, Toronto, ON, Canada. He joined the faculty of the Delft University of Technology, Delft, The Netherlands, in January 2002 as Chair of the Electronics Research Laboratory. His current research interests include: low-power transceiver circuitry for highly integrated wireless applications, and electronics design for high-speed data communications systems.

Prof. Long currently serves on the Program Committees of the International Solid-State Circuits Conference (ISSCC), the European Solid-State Circuits Conference (ESSCIRC), the IEEE Bipolar/BiCMOS Circuits and Technology Meeting (BCTM), and the European Microwave Conference. He is a former Associate Editor of the IEEE JOURNAL OF SOLID-STATE CIRCUITS. He was the recipient of the NSERC Doctoral Prize and Douglas R. Colton and Governor General's Medals for research excellence, and the Best Paper Awards from ISSCC 2000 and IEEE-BCTM 2003.